# Potential of Mean Force Calculation for the Proton and Hydride Transfer Reactions Catalyzed by Medium-Chain Acyl-CoA Dehydrogenase: Effect of Mutations on Enzyme Catalysis†

Sudeep Bhattacharyya,* Shuhua Ma, Marian T. Stankovich,* Donald G. Truhlar,* and Jiali Gao*

*Department of Chemistry, University of Minnesota, Smith Hall, 207 Pleasant Street SE, Minneapolis, Minnesota 55455-0431*

*Received August 16, 2005; Revised Manuscript Received September 27, 2005*

ABSTRACT: Potential of mean force calculations have been performed on the wild-type medium-chain acyl-CoA dehydrogenase (MCAD) and two of its mutant forms. Initial simulation and analysis of the active site of the enzyme reveal that an arginine residue (Arg256), conserved in the substrate-binding domain of this group of enzymes, exists in two alternate conformations, only one of which makes the enzyme active. This active conformation was used in subsequent computations of the enzymatic reactions. It is known that the catalytic α,β-dehydrogenation of fatty acyl-CoAs consists of two C−H bond dissociation processes: a proton abstraction and a hydride transfer. Energy profiles of the two reaction steps in the wild-type MCAD demonstrate that the reaction proceeds by a stepwise mechanism with a transient species. The activation barriers of the two steps differ by only ∼2 kcal/mol, indicating that both may contribute to the rate-limiting process. Thus this may be a stepwise dissociation mechanism whose relative barriers can be tuned by suitable alterations of the substrate and/or enzyme. Analysis of the structures along the reaction path reveals that Arg256 plays a key role in maintaining the reaction center hydrogen-bonding network involving the thioester carbonyl group, which stabilizes transition states as well as the intervening transient species. Mutation of this arginine residue to glutamine increases the activation barrier of the hydride transfer reaction by ∼5 kcal/mol, and the present simulations predict a substantial loss of catalytic activity for this mutant. Structural analysis of this mutant reveals that the orientation of the thioester moiety of the substrate has been changed significantly as compared to that in the wild-type enzyme. In contrast, simulation of the active site of the Thr168Ala mutant shows no significant change in the relative orientation of the substrate and the cofactor in the active site; as a result, this mutation has very little effect on the overall reaction barrier, and this is consistent with the experimental data. This study demonstrates that significant insights into the catalytic mechanism can be obtained from simulation studies, and the results can be used to design novel mechanistic probes for the enzyme.

Mitochondrial β-oxidation has been extensively studied in the past 15 years because a number of mutations in the enzymes (involved in the β-oxidation process) are responsible for diseases related to fatty acid metabolism. Fatty acid metabolism occurs within the mitochondrial matrix and proceeds by a sequence of steps that remove two carbon units in each cycle. The process involves at least 12 different enzymes, including the acyl-CoA[1] dehydrogenases, which are flavoenzymes that perform the first step of this β-oxidation spiral. Members of this group of oxidoreductases act on specific chain lengths of fatty acids, and deficiency in any enzyme of the acyl-CoA dehydrogenase family leads to metabolic diseases. Indeed, a number of mutations have been found in these enzymes in patients who have problems ranging from severe metabolic disorder to cardiac myopathy (*1*).

Medium- and short-chain acyl-CoA dehydrogenases (which hereafter will be called MCAD and SCAD, respectively) are two members of this group, and they catalyze the α,β-dehydrogenation of medium-chain (C4−C14) and short-chain (C4−C6) fatty acyl-CoAs, respectively, by converting them into their corresponding enoyl-CoA forms. They are homologous and share a common functional base, a glutamate (Glu368 for SCAD and Glu376 for MCAD) at the active site. However, the active site cavity of SCAD is much shallower than that of MCAD, consistent with the differing substrate recognizing ability of their active sites (*2*). The substrate activation and catalytic mechanisms are similar in

† This work was partially supported by Grant GM 29344 from the National Institutes of Healths to M.T.S., by Grant GM046736 from National Institutes of Health to J.G., and by NSF Grant CHE03-49122 to D.G.T.

* To whom correspondence should be addressed. S.B.: phone, (612) 624-5257; fax, (612) 626-7541; e-mail, sudeep@chem.umn.edu. M.T.S.: phone, (612) 624-1019; fax, (612) 626-7541; e-mail, stankovi@chem.umn.edu. D.G.T.: phone, (612) 624-7555; fax, (612) 626-9390; e-mail, truhlar@umn.edu. J.G.: phone, (612) 625-0769; fax, (612) 626-7541; e-mail, gao@chem.umn.edu.

[1] Abbreviations: ABNR, adopted basis Newton−Raphson method; CoA, coenzyme A; ETF, electron transfer flavoprotein; FAD, flavin adenine dinucleotide; KIE, kinetic isotope effect; MCAD, medium-chain acyl-CoA dehydrogenase; MD, molecular dynamics; MM, molecular mechanics; PDB, Protein Data Bank; PMF, potential of mean force; QM, quantum mechanics; RMSD, root mean square deviation; SCAD, short-chain acyl-CoA dehydrogenase; SRP, specific reaction parameter.

10.1021/bi051630m CCC: $30.25 
Published on Web 11/24/2005

these enzymes. As the substrates bind to the active site, the substrate thioester carbonyl interacts with the preformed oxyanion hole by two hydrogen-bonding interactions with 2′-OH of FAD and the amide backbone of the glutamate base. These interactions cause polarization of the substrate molecule that is associated with a decrease of the p$K_a$ (*3*) of the acyl-CoA *pro-R* protons and a shift of over 100 mV of the redox potential of the FAD (*4*).

The oxidation of fatty acids occurs at the α- and β-carbons of the acyl-CoA substrate by a formal removal of a hydrogen molecule (*5*). Mechanistically, the process involves a proton abstraction from the α-carbon of the substrate by an active site glutamate residue (Glu376) and a hydride ion transfer from the β-carbon to the cofactor flavin adenine dinucleotide (FAD). Despite extensive experimental studies of various acyl-CoA dehydrogenases, the mechanistic details are still poorly understood, especially as to whether the two steps are concerted or stepwise. In principle, the reaction mechanism (in which two C−H bonds are broken) could be concerted or nonconcerted, with the latter mechanism involving an isolable intermediate. Furthermore, a concerted mechanism can take place synchronously or asynchronously. In the latter case, one bond dissociation largely precedes the other (*5*), but both features correspond to a free energy profile along the reaction coordinate that exhibits only one transition state (i.e., local maximum) or two or more transition states separated by minima corresponding to kinetically insignificant transient species. Strictly speaking, kinetic isotope effects (KIEs) cannot distinguish between a stepwise mechanism and a concerted asynchronous one in which one bond dissociation occurs largely after the variational transition state. However, usually if one observes a KIE for substitution at one but not another bond, it is reasonable to infer a stepwise mechanism with the isotopically sensitive bond broken in the slow step.

Kinetic isotope effects have been determined for a short-chain enzyme (SCAD) in an unpublished thesis with KIEs ranging from 1.2 to 2.2 for different substitutions on butyryl-CoA (*6*). In contrast, for MCAD several studies have been performed, and data from those studies are clearly contradictory. Murfin (*7*), in experiments on the oxidation of hydrocinnamoyl-CoA by MCAD, found a KIE of 6.9 for α$D_2$- and none for β$D_2$-hydrocinnamoyl-CoAs, which indicates a *stepwise* mechanism. However, at high pH, both substitutions resulted in KIEs with values of 3.5, 5.8, and 17 for α$D_2$-, β$D_2$-, and α,β$D_4$-hydrocinnamoyl-CoAs, respectively (*7*). Because the isotope effects appear to be multiplicative rather than additive, these results were interpreted as indicating that the reaction follows a *concerted* mechanism. Kinetic isotope effects of MCAD have also been determined for a different substrate, namely, butyryl-CoA. The KIEs for the α-$D_2$-butyryl-CoA, β-$D_2$-butyryl-CoA, and α,β-$D_4$-butyryl-CoA were found to be 2−3, 14, and 15−28, respectively (*8*, *9*). The KIE of the α-deuterio species appears to be smaller than a typical primary isotope effect (∼5), whereas the observed β-deuterio value is unusually large. These data imply that the β-hydride transfer is slower than the removal of the α-proton, suggesting intermediate stabilization and a nonconcerted mechanism.

Further insight into the SCAD mechanism was provided by a computational approach. The potentials of mean force for SCAD (*10*) in both one and two dimensions indicate that the reaction proceeds through a stepwise mechanism with the β-hydride transfer step as rate-limiting and that both steps contribute to the kinetics (concerted asynchronous or two steps with similar rate constants). Thus it appears that the two most likely possibilities are a concerted asynchronous mechanism or a stepwise mechanism with both steps contributing to the overall rate of the reaction.

In the present work, we use computational methods, similar to that used in SCAD, to shed light on the MCAD mechanism as well as to explore the impact of mutations on catalysis. One of the disease-associated mutations, Thr168Ala, has been chosen for our study. The Thr168 residue is located in the active site of MCAD and has a hydrogen-bonding interaction with the hydride acceptor atom, N5, of the flavin ring of FAD. Biochemical studies show an 80% loss of enzymatic activity in the Thr168Ala mutant, compared to the wild-type enzyme (*11*). Sequence analysis (*2*, *12*) reveals that this threonine is conserved in the flavin-binding domain of these enzymes. Kinetic isotope effects have not been measured for this mutant. To understand the reaction mechanism and the effect of mutation, we employ a computational technique (*10*) similar to that used for the short-chain enzyme to model the medium-chain acyl-CoA and two of its mutant forms.

An earlier report of molecular simulations of MCAD (*13*), starting from the X-ray structure 1EGC (*14*), resulted in an active site conformation that is not suited for modeling the chemical steps of this enzyme. This was due to salt bridge formation between two oppositely charged residues: Arg256, which is conserved in all of the substrate-binding domains of acyl-CoA dehydrogenases (*2*, *12*), and the basic residue, Glu376, that abstracts the α-proton of the substrate. This interaction significantly reduces the basicity of Glu376. In the present work, we started with the PDB structure 3MDE (*15*), and we also observed ion pair formation between Arg256 and Glu376. However, we modified the orientation of the Arg256 (vide infra) by rotating the arginine's guanidinium headgroup by 180° and then performed energy minimization and MD simulations to obtain a conformation suitable for modeling the two reaction steps in MCAD. The resulting configuration is similar to that used in earlier work (*10*) on SCAD. In the course of the calculations, a new structure (PDB code 1UDY) was reported for MCAD (*16*), showing the same Arg256 conformational arrangement that we had arrived at for our simulated active site. This emphasizes the importance of choosing an appropriate starting protein structure for computational simulation of enzymatic reactions.

To probe further the role of Arg256 in transition state stabilization, it was computationally replaced by a glutamine. Using a combined quantum mechanical and molecular mechanical (QM/MM) potential (*17*−*19*), we then carried out molecular dynamics (MD) simulations (*17*, *20*, *21*) of both catalytic steps of the wild-type enzyme and the two mutants (Thr168Ala and Arg256Gln) of MCAD.

## MATERIALS AND METHODS

All computations were carried out using the computer program CHARMM (C28a3) (*21*) along with CHARMM22 (*22*, *23*) all-atom force field for the enzyme, substrate, and cofactor. The three-point-charge TIP3P model (*24*) was used

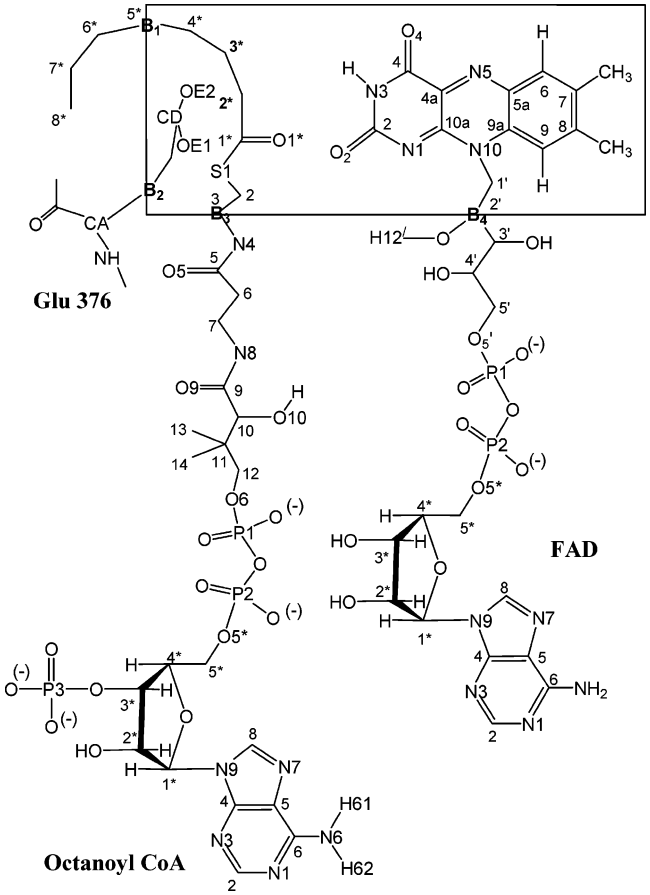


FIGURE 1: Representation of the cofactor FAD, substrate octanoyl-CoA, and base Glu376 in the active site of MCAD. Quantum mechanically treated atoms are shown inside a rectangle. Four $sp^3$ carbon atoms, represented as B1, B2, B3, and B4, are taken as boundary atoms. In the QM/MM method used in this study, boundary atoms are partly quantum mechanical and partly molecular mechanical. Most hydrogen atoms bonded to carbon are omitted in the figure for clarity.

to represent solvent water. Nonbonded interactions were truncated using a switching function between 11 and 12 Å, and the dielectric constant was set to unity. Bond lengths and bond angles of water molecules and bonds involving a hydrogen atom in the protein were constrained by the SHAKE algorithm (*25*). In all molecular dynamics simulations, a time step of 1 fs was used in the leapfrog Verlet algorithm for integration (*26*, *27*).

*Ternary Enzyme−Substrate−Cofactor Complex*. The protein coordinates (PDB code 3MDE) (*15*) were obtained from the Protein Data Bank (*28*). The coordinates represent a homodimeric structure of the enzyme. However, since the tetramer is the active form for this group of enzymes (including MCAD), we constructed the tetramer configurations by crystal symmetry operations using the CRYSTAL BUILDER module of Cerius2 (Accelrys Inc.). The tetrameric structure was used in subsequent calculations. All water molecules associated with the dimeric structure of the protein determined X-ray crystallographically were retained in both dimeric components of the tetramer. Each of the four subunits has an active site, which could in principle contain a substrate (octanoyl-CoA) and a cofactor (FAD). Since each active site functions independently, we chose to limit our computation to a single active site, occupied by one octanoyl-CoA and one FAD molecule; the other three binding pockets were

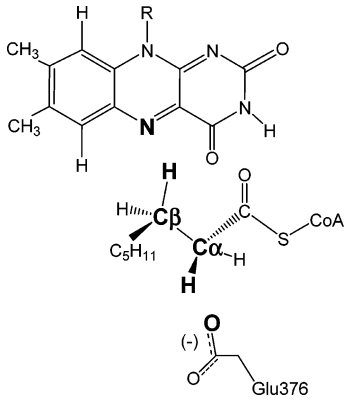


FIGURE 2: Representation of atoms used in defining the reaction coordinates for the proton and hydride transfer reactions. As described in Materials and Methods, six atoms, Cα, H, O, C$\beta$, H, and N (shown in bigger and bold fonts), have been used in defining the two reaction coordinates, $z_1$ and $z_2$.

left empty. The arginine residue at the active site, Arg256, was oriented so that its interaction pattern matched closely with the active site of the short-chain enzyme as reported in the crystal structure of PDB code 1JQI (*29*) and in a previous simulation (*10*). For studying the Thr168Ala and Arg256Gln mutated structures, point mutations were made by replacing Thr168 and Arg256 by Ala168 and Gln256, respectively. All of these manipulations were accomplished with the aid of graphics visualization.

*Hydrogen Addition and Modeling Charged Residues*. The hydrogen atoms were added by using the HBUILD module of CHARMM (*21*). All ionic amino acid residues were kept in a protonation state corresponding to pH 7. Histidine residues were modeled as neutral, and the question whether the proton will be located on N$\epsilon$ or N$\delta$ of a particular imidazole moiety was answered by considering the possible hydrogen-bonding network of the atoms in that residue with its neighboring atoms in the X-ray crystallographic structure (*15*). The protonation states of all of the histidine residues deduced in this way were consistent with the assumption that they are neutral. The active site base Glu376, which abstracts the α-proton, was deprotonated.

*Representation of Atoms*. The protein−substrate−cofactor system was partitioned into two zones. Atoms that are in or close to the active site were treated quantum mechanically. A total of 55 atoms (shown in the rectangular box in Figure 1) were included in the quantum mechanical region, where boundary atoms that are treated partly quantum mechanically and partly classically are counted as QM atoms. The QM subsystem consists of the entire isoalloxazine ring and up to the second ribityl carbon attached to the N10 of FAD. In octanoyl-CoA, the QM region included the C$\delta$(C5*), C$\gamma$(C4*), C$\beta$(C3*), and Cα(C2*) atoms of acyl chain and the carbonyl carbon (C1*) and carbonyl oxygen (O1*), and it extends up to the amino-functionalized carbon of the $\beta$-meracaptoethanolamine moiety. Also, a part of the side chain of Glu376 was included in the QM region (Figure 2). The rest of the atoms in the molecule constitute the MM region. Four $sp^3$ carbon atoms (represented as B1, B2, B3, and B4 in Figure 2) joining the QM and MM region were treated with generalized hybrid orbitals (*18*, *19*).

*Potential Energy Functions*. Quantum mechanical calculations on the QM region (described above) were carried out

using the semiempirical Austin model 1 (AM1) method (*30*). As described in the previous report (*10*), for accurately determining the barrier height of the proton and hydride transfer reactions, modifications were made in the AM1 parameters to match the energy of reaction for the proton transfer process with that from Gaussian-3 (*31*, *32*) calculations. Thus, specific reaction parameters (SRP) (*33*) were used. In particular, the parameter $U_{pp}$ for the two Glu376 carboxylate oxygen atoms was modified, while the rest of the AM1 parameters were kept unchanged. For the hydride transfer, a simple valence bond (SVB) term (*34*) was added and calibrated to the barrier height obtained by constrained ab initio optimizations (*10*). The form and parameters of the SVB potentials have been reported previously (*10*). The final potential surface described by the hybrid QM(AM1-SRP + SVB)/MM potentials is therefore

$$V = V_{\mathrm{QM(AM1-SRP)/MM}} + V_{\mathrm{SVB}} \quad (1)$$

*Boundary Conditions.* We used stochastic boundary conditions (*35*) in the calculations. In this procedure, the system is divided into three regions: the reaction zone, the Langevin region (also called the buffer zone), and the reservoir zone. The reaction zone consists of all atoms within a radius of 24 Å of the reaction center, defined as the average of the coordinates of all 55 atoms in the QM region, and is treated by Newtonian mechanics. Atoms within a 24−30 Å shell are designated as a buffer zone. The atoms in this region act as a heat bath and are treated by the Langevin equations of motion by imposing a friction force and a random force on non-hydrogenic atoms in this region. The friction coefficients for this computation were maintained at 200 $ps^{-1}$ for all protein atoms and 62 $ps^{-1}$ for the water atoms in the buffer region. Furthermore, a harmonic restraining function was imposed on the buffer atoms to allow the system to maintain its structural integrity. At the outer edge of the buffer zone, the values of the harmonic force constants used were 1.22 kcal $mol^{-1}$ $Å^{-2}$ for main-chain oxygen atoms, 1.30 kcal $mol^{-1}$ $Å^{-2}$ for all other main-chain atoms, and 0.73 kcal $mol^{-1}$ $Å^{-2}$ for all atoms of side-chain and water molecules. From the outer toward the inner Langevin region, the harmonic force constants are gradually scaled to zero at the reaction region boundary. The remaining atoms within 45 Å are in the reservoir zone, whereas atoms beyond 45 Å were deleted. The system had a total of 22667 atoms, with 7783 atoms in the reactant zone, 6230 in the buffer zone, and 8654 atoms in the reservoir zone. Of the 7783 atoms in the reaction zone, there are 103 substrate atoms, 84 cofactor atoms, 5472 protein atoms, and 2124 water atoms.

*Solvent Addition*. We have kept all water molecules originally determined in the X-ray structure in the enzyme−cofactor−substrate ternary complex. This structure was further solvated by placing the geometric center of the protein−substrate−cofactor system at the center of a cubic box ($60 \times 60 \times 60$ $Å^3$) of water, previously equilibrated by molecular dynamics simulations. Water molecules from the water box were retained within 30 Å from the center. Water molecules that were within 2.5 Å of any non-hydrogenic atoms were removed. This operation was repeated four times by rotating the water cube along a randomly chosen axis. To relax unfavorable contacts, the system was simulated in 5 ps of MD calculations. The cycle of 4-fold superposition, deletion, and rotation was used to fill in any cavity generated during the equilibration.

*Equilibration and Structure Engineering*. After the solvated ternary complex was obtained, energy minimizations were performed to remove close contacts prior to the heating simulation. The minimization was carried out in two steps. Initially, only the energy of the atoms within the QM region was minimized using 40 steps of the adopted basis Newton−Raphson (ABNR) minimization algorithm. Next, an additional 100 cycles of ABNR minimization were carried out by fixing the quantum mechanical atoms and all of the atoms beyond 30 Å of the active site center, including the main-chain carbon and nitrogen atoms and the water molecule atoms.

Then the system was gradually heated in four cycles of 5 ps each from 20 to 300 K. As described in the subsection Ternary Enzyme−Substrate−Cofactor Complex, in the wild-type and Thr168Ala MCAD structures, the active site was engineered with a modification of the Arg256 orientation in the active sites. Additionally, in Thr168Ala, the threonine group was replaced by an alanine. After these modifications the active site was further equilibrated in each case before proceeding to further simulations. This was accomplished in the following steps. First, the active site structures of both enzymes, MCAD (PDB code 3MDE) (*15*) and SCAD (PDB code 1JQI) (*29*), were analyzed to identify a number of interacting atom pairs, critical in retaining the active site conformation of the respective enzymes. MD simulations were performed on the modified active site (which was now a hybrid of the two above-mentioned structures) by applying harmonic constraints on these pairs of atoms. Each of these constrained initial MD simulations consisted of 20 ps heating and 30 ps equilibration steps. Finally, all of these constraints were removed, and the system was further equilibrated for 30 ps of MD simulation. After each step, the active site structures were visualized, and the relative orientations of Arg256, Glu376, and the thioester moiety were studied. The best structure obtained in this way was used as a starting point for simulating the enzymatic reaction steps.

*Potential of Mean Force Sampling*. The potential of mean force (PMF) was calculated for the equilibrated system as a function of the reaction coordinate. The reaction coordinates for each of the two reactions (proton transfer and hydride transfer) are defined as $z = r_{\mathrm{break}} - r_{\mathrm{form}}$, where each $r$ is an internuclear distance which will now be defined using Figure 2. For α-proton abstraction the reaction coordinate, $z_1$, is chosen as $r_{C\alpha H} - r_{OH}$, which is the difference between the Cα−H distance and the O−H separation. Similarly, the $\beta$-hydride reaction coordinate, $z_2$, is equal to the difference between the interatomic distances $r_{C\beta H}$ and $r_{NH}$. For each reaction step, the range of the reaction coordinate was divided into several individual simulations, called "windows", in each of which we added a biasing line potential that roughly mirrors the PMF and a harmonic restraining force centered at the central location ($z_i^0$) of that particular window. The biasing potential was adjusted on the basis of the initially computed PMF during the equilibration stage of the umbrella-sampling simulations. In each window, the system was equilibrated for 25 ps, and then the configurations along $z$ were sampled for 50 ps to yield the PMF; the coordinates were saved on every 100th step. Velocities and positions of the final configuration generated by a particular window were

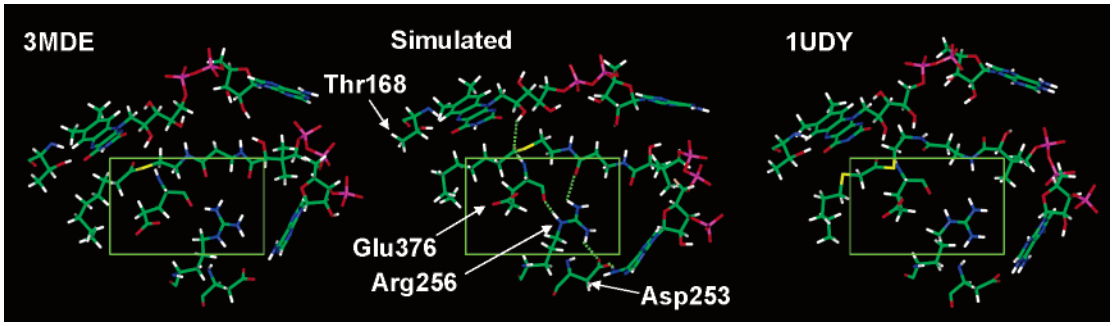


FIGURE 3: Comparative structural representation of the active sites in crystal structures (PDB structures 3MDE and 1UDY) and the equilibrated model in this work, showing the respective orientations of Arg256 and Glu376 in rectangular boxes.

used to initiate the computation in the next window. Free energy as a function of the reaction coordinate was obtained by using the umbrella-sampling technique (*36*, *37*). In particular, the weighted histogram analysis method (WHAM) (*36*, *38*) was used to obtain the unbiased free energy profile for the reaction. The PMF at the reactant side for the proton abstraction simulation was anchored at zero, while for the hydride transfer the starting value of the PMF was set equal to the energy of the product of the proton transfer reaction.

## RESULTS AND DISCUSSION

*Conformations of Arg256*. A number of structures have been determined experimentally for this group of enzymes (*14*−*16*, *29*, *39*, *40*), and although the overall structures are very similar, with RMSD values of 0.3−0.5 Å, there is a significant difference in the conformation of the Arg256 residue at the substrate-binding site. Arg256 is completely conserved in acyl-CoA dehydrogenases (*2*, *12*) and plays a critical role in binding substrate. In the available X-ray crystal structures, two different conformations of this arginine were observed. In the structures of medium-chain enzymes [PDB structures 3MDE (*15*) and 1EGC (*14*)], the arginine N$\epsilon$ atom is directed toward the Asp253 (Figure 3). However, in the short-chain acyl-CoA dehydrogenase structures [PDB structures 1JQI (*29*) and 1BUC (*40*)] the orientation of the arginine was found to be significantly different. In particular, the respective arginine's N$\epsilon$ atom is flipped 180° and makes a hydrogen-bonding contact with the backbone carbonyl group of the Glu367.

When we performed simulations using the arginine configuration in the 3MDE structure (which is of the former type), it led to an ion pair interaction between Arg256 and Glu376. The latter residue is the putative base in the proton abstraction step, and the ion pair with Arg256 severely reduces its proton abstraction ability needed for catalysis. A previous simulation (*13*) of the active site starting with a different structure (PDB structure 1EGC) (*14*) also led to the Arg256−Glu376 salt bridge, and it was concluded that the active site conformation of 1EGC is not the correct conformation for enzymatic catalysis (*13*). On the other hand, in the short-chain enzyme, when computational models were constructed starting with the flipped orientation of the arginine (as they appear in PDB structures 1BUC or 1JQI), this ion pair interaction was not observed (*10*, *41*) as a dominant configuration.

Thus, in the present study, we flipped the arginine's guanidinium moiety to mimic the configuration in the SCAD active site (PDB structures 1JQI and 1BUC). The modification introduced by altering the orientation of Arg256 did not introduce major conformational changes in the active site, including the acyl group, the thioester moiety, the panthothenate carbonyls (anchored to Arg256), and the phospho-ADP of the acyl-CoA, as compared to the original structure in 3MDE. The system was then further equilibrated by combined QM/MM simulations for 30 ps, and it was found that the relative orientations of the active site base Glu376, octanoyl-CoA (the proton and hydride donor substrate), and FAD (the hydride acceptor) are retained [as compared to the starting crystal structure in 3MDE (*15*)]. The interactions between Arg256 and Glu376 are now weakly coupled, resembling the active site of the short-chain enzyme (1JQI) (*29*). While this work was still in progress, the existence of this flipped conformation of Arg256 in MCAD was confirmed by a recent crystal structure (*16*) (1UDY) that contains a substrate analogue, 3-thiaoctanoyl-CoA molecule (Figure 3). Thus, the two X-ray structures (3MDE and 1UDY) represent distinct active site configurations with differing Arg256 conformations, and our simulation results indicate that only one of them corresponds to a functionally active enzyme.

*Potential of Mean Force*. Previous studies of the SCAD oxidation reaction (*10*) demonstrated that the coupled proton and hydride transfer reactions have a stepwise character with an enolate anion transient species between the two steps. If this transient species has a long enough lifetime, it could be an observable intermediate, but we did not predict the lifetime, and it has not been observed experimentally; therefore, we will call it a transient species. If it lives long enough to be a stabilized intermediate, one should observe nonconcerted kinetics. On the other hand, if it lives too fleetingly to be thermalized, the kinetics may be concerted with nonsynchronous atomic motions. When we call the process stepwise, we do not distinguish between nonconerted and nonsynchronous. A definitive comparison to experiment would require further work on the effect of changing substrate and pH, and thus the correspondence to the KIE experiments requires further study. Nevertheless, the theoretical prediction of stepwise character of the atomic motions provides a framework for further discussion. The conclusion that the atomic motion is stepwise was confirmed by both one- and two-dimensional potentials of mean force associated with the two reaction coordinates. The computed primary KIEs are also consistent with this mechanism, and the values are in accord with the experimental data. In the present calculations of the MCAD system, we adopted the stepwise reaction mechanism to initiate the work and the reasonable-

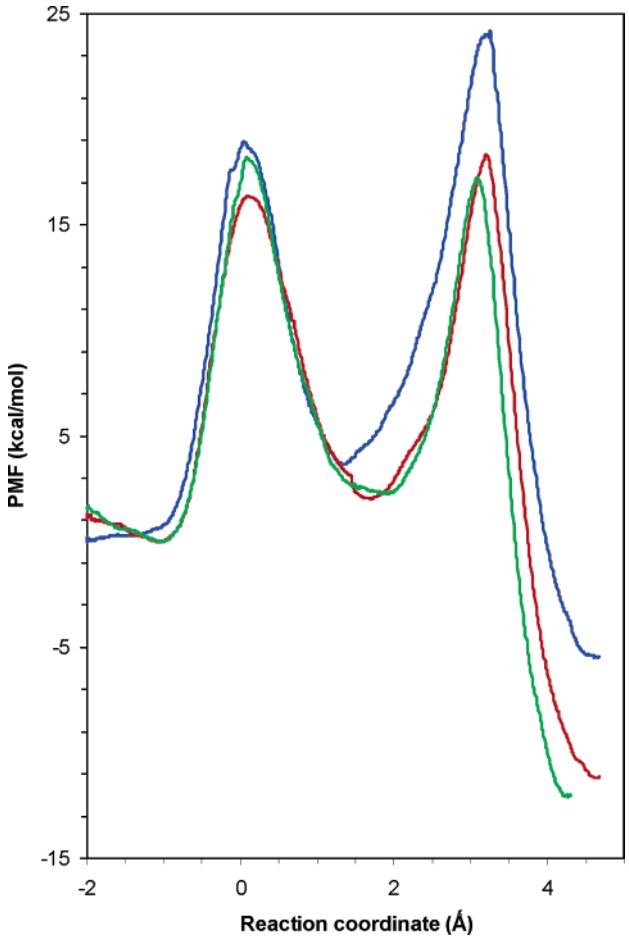


FIGURE 4: Potentials of mean force for the wild-type (red) enzyme and for the Thr168Ala (green) and Arg256Gln (blue) mutants. The two reaction coordinates are placed end to end for this figure. The reaction coordinate of the proton transfer is on the left, and the reaction coordinate of the hydride transfer reaction is shifted to the right by 3.45, 3.45, and 3.15 Å for the wild-type, Thr168Ala, and Arg256Gln enzymes.

ness of this adoption is confirmed by the results presented in this section.

Potentials of mean force were computed for the proton and hydride transfer reactions of the wild-type MCAD and the Arg256Gln and Thr168Ala mutants, all at 298 K. In the proton transfer step, Glu376 abstracts a *pro-R* α-proton from the octanoyl-CoA substrate, resulting in an enolate ion transient species. This is followed by the second step, where the *β*-hydride is transferred onto the N5 atom of the flavin along with Cα−C*β* double bond formation in the substrate. The free energy profiles were determined along the reaction coordinate, $z_1$, for the proton transfer reaction, and $z_2$, for the hydride migration ($z_1$ and $z_2$ are defined in Materials and Methods). In each case, the product configuration of the first reaction step, i.e., the proton abstraction reaction, was used as the starting structure for the *β*-hydride transfer step. The free energy of the reactant of the second reaction step was made equal to that of the product of the proton transfer step reaction. A total of 1.5 ns of simulations was performed for the combined proton and hydride transfer reactions in each case (the wild-type enzyme and its mutants). The results are shown in Figure 4.

*(A) Wild-Type MCAD*. The potential of mean force in Figure 4 shows that the two reaction steps are stepwise with the formation of an enolate ion transient species. This confirms that our initial computational strategy is valid. In the wild-type MCAD, the observed barriers for the two reaction steps are similar, with a value of 16.4 kcal/mol for the proton abstraction and 18.2 kcal/mol for the hydride transfer. The transient species structure has a free energy minimum that is only ∼2 kcal/mol higher than that of the Michaelis complex (Figure 4). The small difference of 1.8 kcal/mol between the two reaction barriers, which is close to the uncertainties of our computational results, suggests that both steps contribute to the overall rate of the reaction and may be partially rate determining.

*(B) Thr168Ala Mutant*. The free energy profile for the disease-associated mutant Thr168Ala shows that the α-proton and *β*-hydride transfer reactions have energy barriers of 18.2 and 17.2 kcal/mol, respectively (Figure 4). The proton transfer step increases by 2 kcal/mol compared to the wild-type enzyme, while the hydride transfer barrier decreases by 1 kcal/mol. Thus the overall barrier remains the same, ∼18.2 kcal/mol, but the mutation will make the proton transfer reaction slower compared to that in the wild type. The proton transfer step is predicted to make a greater contribution to limiting the rate of the overall reaction than in the wild-type case. The transient species has a stabilization energy identical to that observed for the wild-type enzyme, and again a stepwise mechanism is predicted.

Quantitatively, the canonical unified statistical theory (*42*, *43*) shows that the combination of 18.2 and 16.4 kcal/mol free energy barriers corresponds to a phenomenological free energy barrier of 18.23 kcal/mol, whereas the combination of 18.2 and 17.2 kcal/mol barriers corresponds to a phenomenological free energy barrier of 18.30 kcal/mol or a slower rate than that of the former two-barrier case by 13%. The activity, determined experimentally by a ferricinium assay of this mutant enzyme, was reduced by only 80% of that of the wild type (*11*). This translates to an increase in the phenomenological free energy of activation by less than 1 kcal/mol. Thus, the simulation results are consistent with the experimental data.

*(C) Arg256Gln MCAD*. The free energy profile of the Arg256Gln mutant shows (Figure 4) that the transient species is less stable compared to that in the wt and Thr168Ala MCAD and is 5 kcal/mol higher than the reactant state. This indicates an increase of ∼2 kcal/mol in the free energy for the proton transfer reaction in this mutant. However, the reaction is still predicted to be stepwise.

Thus the energy barriers for both steps are increased due to the mutation. Compared to the wild-type enzyme, the activation barrier for the proton transfer step is elevated by 3 kcal/mol. However, the effect of the mutation is more pronounced in the *β*-hydride transfer step, whose barrier height exhibits an increase of about 5 kcal/mol (Figure 4). The overall barrier height is thus increased by the same amount, indicating a $10^4$-fold reduction of the activity of the Arg256Gln mutant. The PMF calculation also reveals that the catalytic role of Arg256 is stronger for the hydride transfer reaction step than the proton one, so much so, in fact, that without Arg256 the hydride transfer step is rate-limiting for the Arg256Gln mutant enzyme.

Thus our computations indicate that this mutation severely inactivates the enzyme. While this paper was in preparation, this prediction was confirmed by a recent report of an

Table 1: Selected Hydrogen-Bonding Interactions of the Substrate (Octanoyl-CoA) and the Cofactor (FAD) with the Neighboring Residues of wt MCAD and Its Mutants[a]

| molecule/hydrogen bonds | 3MDE crystal structure (Å) | equilibrated MCAD structure (Å) | equilibrated T168A-MCAD (Å) | equilibrated R256Q-MCAD (Å) |
|---|---|---|---|---|
| FAD:N5−Thr168:HG1 | 2.0 | 2.3 | | 2.4 |
| FAD:O4−Thr168:HN | 2.3 | 1.9 | 3.3 | 2.0 |
| FAD:N5−Thr168:HN | 3.0 | 2.6 | 2.8 | 2.4 |
| FAD:HN3−Tyr133:O | 1.9 | 2.0 | 2.0 | 1.9 |
| FAD:O2−Val135:HN | 2.2 | 2.2 | 2.0 | 2.4 |
| FAD:O2−Thr136:HN | 2.0 | 2.3 | 1.8 | 2.0 |
| FAD:N1−Thr136:HG1 | 1.8 | 2.7 | 2.0 | 2.2 |
| FAD:H12′−CoA:O1* | 2.1 | 2.4 | 2.8 | 3.8 |
| CoA:O−Glu376:HN | 2.2 | 2.1 | 2.4 | 4.6 |
| Glu376:O−Arg256[b]:HE | 2.3 | 2.3 | 3.7 | 2.0 |
| Glu376:O−Lys333:HZ1 | 2.9 | 3.6 | 3.6 | 4.6 |
| CoA:O5−Arg256:HH22 | 2.6 | 2.5 | 3.1 | |
| CoA:O9−Arg256:HH21 | 3.7 | 4.4 | 1.9 | |
| Arg256:HH12−Asp253:OD1[b] | 3.9 | 2.9 | 4.4 | |
| Asp253:OD2−CoA:H62 | 2.3 | 2.3 | 2.3 | 2.2 |

[a] The distances tabulated are from the proton to the acceptor oxygen or nitrogen atom. [b] The orientation of Arg256 in the simulated structure of MCAD and 3MDE differs such that the guanidinium protons that interact with the Glu376 carbonyl oxygen and pantothenate carbonyls of octanoyl-CoA are different. In each case the distance from the nearest protons is measured for the hydrogen bond comparison.

experimental study with Arg256Gln MCAD by Zeng et al. (*44*). The overexpressed recombinant mutant enzyme was found to possess no catalytic activity. Thus our computations indicate that this mutation severely inactivates the enzyme.

*Hydrogen-Bonding Interactions and Their Changes along the Reaction Coordinates of Proton and Hydride Transfer*. MCAD is a medium-sized homotetramer, which has a molecular mass of 44 kDa per monomer (*15*). The substrate octanoyl-CoA binds in a cavity adjacent to the isoalloxazine ring of the FAD cofactor and has hydrogen-bonding contacts with the ribityl hydroxyl (2′-OH) group of the cofactor. Experimental studies (*45*−*48*) show that hydrogen-bonding interactions play significant roles in activating the enzyme by guiding the orientations of the cofactor (FAD), the substrate, octanoyl-CoA (referred as CoA for describing the hydrogen bonding in Tables 1 and 2), and the proton-abstracting base (Glu376). Furthermore, several hydrogen-bonding contacts in the reaction center are responsible for stabilizing the transition states for both reaction steps. An extended hydrogen-bonding interaction network involving FAD, octanoyl-CoA, and Glu376 along with several active site residues is clearly identifiable, as shown in Figure 5. Table 1 shows the hydrogen-bonding interactions obtained from the crystal structure, which are compared with the average hydrogen-bonding distances of the present simulations of the wild-type enzyme and the two mutant forms.

*(A) Wild-Type Enzyme*. In the wild-type enzyme, the crystal structure (*15*) shows that the FAD cofactor is bound tightly in the active site. The tricyclic isoalloxazine ring of the FAD has been implicated to play a significant role in the folding of this enzyme (*49*), and it makes a number of hydrogen-bonding contacts with the active site residues. A threonine (Thr168) residue interacts with the N5 (hydride acceptor) and O4 atoms of the flavin ring through two well-formed hydrogen bonds: FAD:N5−Thr168:HG1 (2.3 Å) and FAD:O4−Thr168:HN (1.9 Å) (Figure 5 and Table 1). The other isoalloxazine ring atoms, N3, O2, and N1, interact with polar Tyr133 and Thr136 groups, forming three more hydrogen-bonding interactions, namely, FAD:HN3−Tyr133:O (2.0 Å), FAD:O2−Thr136:HN (2.3 Å), and FAD:N1−Thr136:HG1 (2.7 Å) (Table 1). The backbone amide of a neutral residue, Val135 (not shown), also interacts with flavin atom O2 through (FAD:O2−Val135:HN, 2.2 Å).

The thioester moiety of octanoyl-CoA is bound to the active site pocket by virtue of two hydrogen-bonding contacts (Figure 5) with the ribityl 2′-hydroxyl group (FAD:H12′−CoA:O1*, 2.4 Å) and the Glu376 backbone amide (Glu376:NH−CoA:O1*, 2.1 Å) (*15*). These two hydrogen-bonding interactions resemble features observed in the oxyanion stabilization in the peptide hydrolysis by serine protease, although the latter consists hydrogen bonds donated from two backbone amide groups (*48*, *50*).

A network of hydrogen-bonding interactions, starting from this reaction center (thioester carbonyl), passes through residues Glu376, Arg256, and Asp253 to reach the adenosine end of the octanoyl-CoA (Table 1 and Figure 5). Arg256 occupies a position that is geometrically centered in the network. The HE atom of Arg256 is hydrogen bonded to the backbone carbonyl of the base Glu376 through Arg256:HE−Glu376:O (2.3 Å). Also, Arg256 is involved in the binding of the octanoyl-CoA and makes moderate interactions with the pantothenate carbonyl oxygens O5 and O9, as reflected from the distances of CoA:O5−Arg256:HH22 (2.5 Å) and CoA:O9−Arg256:HH21 (4.4 Å). The network of interaction extends up to the phosphoadenosine end of the substrate through two more hydrogen bonds: Arg256:HH12−Asp253:OD1 (2.9 Å) and Asp253:OD2−CoA:H62 (2.3 Å) (Table 1 and Figure 5).

Table 2 shows that most of the hydrogen-bonding contacts of the isoalloxazine ring did not undergo any significant change in the course of our simulations of the two reactions. Hydrogen-bonding interactions of the flavin ring with Thr136 and Thr168 were maintained, and they remained quite invariant along the reaction coordinates of both α-proton abstraction and *β*-hydride transfer reactions.

The variations of hydrogen-bonding interactions along the reaction pathways reveal that the reaction center thioester carbonyl moiety maintains two hydrogen-bonding interactions with ribityl 2′-OH of FAD (FAD:H12′−CoA:O1*) and the backbone amide group of Glu376 (CoA:O1*−Glu376:HN) throughout both reaction steps (Figures 5−7). An interesting observation in this analysis is the nature of the evolution of the enolate ion at the end of the proton transfer reaction. The buildup of negative charge on the oxygen (O1*) is clearly indicated by the strong decrease (Figure 6) of the two hydrogen-bonding interaction distances with this atom, during the first reaction step. Then the hydride transfer step removes the enolate functionality, and this is also reflected in the increase in hydrogen-bonding distances of these interactions (Figure 7). The interaction of the Glu376 carbonyl group with the HE atom of Arg256 was also maintained throughout the first reaction profile. The phosphoadenosine end of octanoyl-CoA interacts quite strongly with Asp253, and the distance of Asp253:OD2−CoA:H62 remains almost invariant (1.7−1.8 Å) throughout the two reactions.

Table 2: Comparison of the Selected Hydrogen-Bonding Interactions for Reactant, Transition State 1, Intermediate, Transition State 2, and Product As Observed in the Active Site of wt, Thr168Ala, and Arg256Gln Mutants Equilibrated and Through the Reaction Coordinate

| | proton and hydride transfer | | | | | | | | | | | | | | |
|---|---|---|---|---|---|---|---|---|---|---|---|---|---|---|---|
| | wt MCAD | | | | | Thr168Ala MCAD | | | | | Arg256Gln MCAD | | | | |
| hydrogen bonds | R (Å) | TS1 (Å) | Int (Å) | TS2 (Å) | Pr (Å) | R (Å) | TS1 (Å) | Int (Å) | TS2 (Å) | Pr (Å) | R (Å) | TS1 (Å) | Int (Å) | TS2 (Å) | Pr (Å) |
| FAD:N5−Thr168:HG[a] | 2.3 | 2.4 | 2.2 | 2.2 | 2.2 | | | | | | 2.2 | 2.3 | 2.3 | 2.4 | 2.3 |
| FAD:O4−Thr168:HN | 2.0 | 2.0 | 2.0 | 2.0 | 2.0 | 3.3 | 2.4 | 3.8 | 2.2 | 2.1 | 2.0 | 2.0 | 2.0 | 2.0 | 2.0 |
| FAD:N5−Thr168:HN | 2.9 | 2.9 | 3.0 | 3.1 | 3.3 | 2.9 | 2.7 | 3.2 | 3.0 | 2.9 | 3.1 | 3.0 | 3.0 | 3.7 | 3.3 |
| FAD:HN3−Tyr133:O | 1.9 | 2.0 | 1.9 | 1.9 | 2.0 | 1.8 | 1.8 | 1.8 | 1.9 | 1.9 | 1.9 | 1.9 | 1.9 | 1.9 | 1.9 |
| FAD:O2−Thr136:HN | 2.1 | 2.1 | 2.1 | 2.0 | 2.0 | 2.0 | 2.0 | 2.0 | 1.9 | 2.4 | 2.0 | 2.0 | 2.0 | 2.0 | 2.0 |
| FAD:N1−Thr136:HG1 | 2.9 | 2.9 | 3.2 | 2.2 | 2.0 | 2.4 | 2.3 | 2.3 | 2.8 | 3.9 | 2.7 | 2.5 | 2.4 | 2.1 | ‘2.0 |
| CoA:O1*−FAD:H12′ | 2.4 | 2.0 | 1.9 | 2.0 | 2.1 | 3.7 | 3.1 | 2.0 | 3.2 | 3.9 | 3.8 | 4.6 | 4.5 | 4.4 | 4.3 |
| CoA:O1*−Glu376:HN | 2.2 | 2.0 | 1.9 | 2.0 | 2.1 | 2.1 | 2.1 | 2.0 | 2.2 | 2.1 | 4.7 | 4.8 | 4.4 | 5.3 | 4.6 |
| Glu376:O−Arg256:HE[b] | 3.3 | 2.4 | 2.4 | 2.3 | 4.1 | 3.5 | 3.5 | 3.5 | 3.7 | 3.8 | 2.1 | 2.5 | 2.0 | 1.9 | 2.1 |
| CoA:O5−Arg256:HH22 | 4.0 | 2.7 | 2.6 | 2.5 | 3.4 | 3.6 | 2.8 | 2.3 | 3.5 | 3.6 | | | | | |
| CoA:O9−Arg256:HH21 | 4.2 | 4.2 | 4.4 | 4.0 | 4.0 | 2.2 | 2.2 | 2.7 | 2.4 | 2.5 | | | | | |
| CoA:H62−Asp253:OD2 | 1.8 | 1.7 | 1.8 | 1.7 | 1.7 | 2.5 | 2.0 | 2.0 | 2.0 | 3.0 | 3.6 | 3.1 | 3.3 | 3.0 | 3.4 |

[a] In the Thr168Ala mutant the distance of the backbone amide of Ala168 is measured from O4 and N5 of the flavin ring. [b] In the Arg256Gln mutant the distance of the closest amide proton of Gln256 is measured from the backbone carbonyl of Glu376.

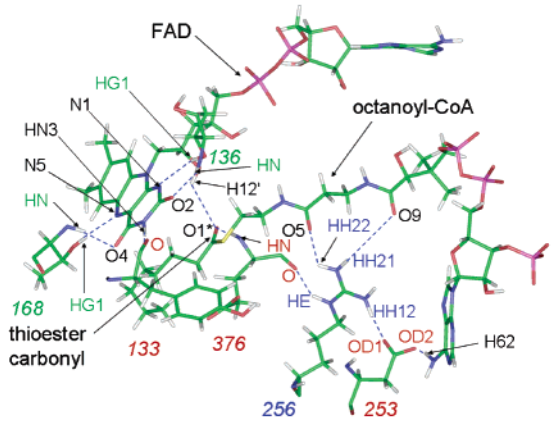


FIGURE 5: Hydrogen-bonding network with the cofactor, FAD, and the substrate, octanoyl-CoA, in the equilibrated wt MCAD active site. Enzyme residue numbers are shown in italics and colored. Colored atom labels correspond to the following residues: Thr136 and Thr168 (green); Tyr133, Glu376, and Asp253 (red); Arg256 (blue); octanoyl-CoA and FAD (black).

This analysis of the evolution of the interactions indicates that Arg256 plays a central role in the hydrogen-bonding network that encompasses the reaction center at the thioester of the substrate. The variations of all of the hydrogen-bonding interactions (Figures 6 and 7 and Table 2) with Arg256 further suggest that despite the fact that Arg256 can rotate, it maintained a single conformation throughout the two simulated reaction steps. The persistence of all these hydrogen-bonding interactions throughout the two reaction steps is indicative of their collective role in maintaining the active site geometry and thus contributing to the stabilization of the transition states, the transient species, and the product states. This catalytic role explains why this residue is highly conserved.

*(B) Thr168Ala MCAD*. The absence of the hydroxyl group in Ala168 reduces its interactions with the flavin ring atoms, N5 and O4. The weaker interaction of the backbone amide of Ala168 with the flavin O4 atoms is reflected in an increase in the FAD:O4−Ala168:HN distance by about 1.5 Å (Figures 6 and 7) as compared to the wild-type enzyme. No significant difference is observed for any of the other hydrogen-bonding interactions with the isoalloxazine ring. The mutation of

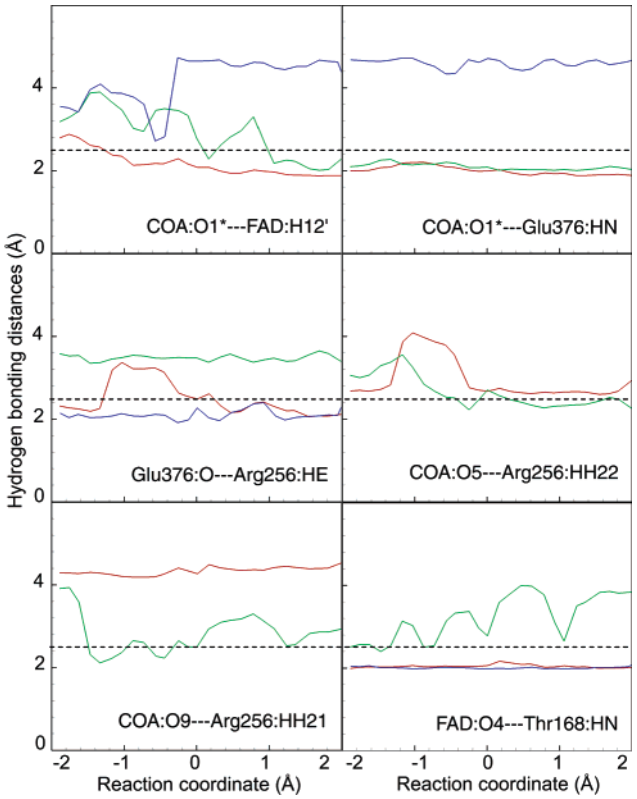


FIGURE 6: Variation of selected hydrogen-bonding distances of FAD and octanoyl-CoA along the proton transfer reaction coordinate in the wt (red) and in the Thr168Ala (green) and Arg256Gln mutants of MCAD (blue). Dotted lines at 2.5 Å indicate the formation and breaking of hydrogen bonds.

Thr168Ala has little effect on the hydrogen-bonding interactions of the thioester carbonyl (O1*) (Figures 6 and 7). Of the two hydrogen-bonding interactions, only one changes significantly; in particular, the CoA:O1* −FAD:H12′ (with the 2′-ribityl hydroxyl group as shown in Figure 4) increased by 1.0 Å, compared to wt MCAD. However, Arg256 appears to have moved away from the base Glu376 in this mutant. This is evident from an increase of ∼1.0 Å in the Glu376:O−Arg256:HE distance and a decrease of ∼1.5 Å in the CoA:O9−Arg256:HH21 distances (Figure 5), compared to that in the wild type (Tables 1 and 2 and Figures 6 and 7).

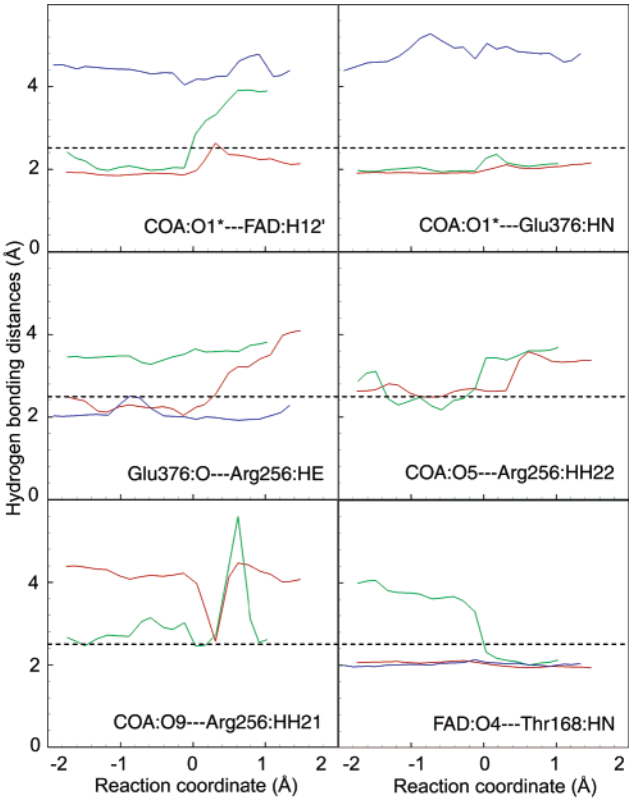


FIGURE 7: Variation of selected hydrogen bond distances along the reaction coordinate of the hydride transfer reaction for the three enzymes, with the same color codes as used in Figure 6. Dotted lines at 2.5 Å indicate the formation and breaking of hydrogen bonds.

This is also reflected in the results of structure comparison of the active sites for these two proteins (vide supra).

Sequence and structure comparison studies (*2*) of acyl-CoA dehydrogenases with acyl-CoA oxidases suggest that although the latter enzymes lack Thr168, they successfully carry out the same α,*β*-dehydrogenation of acyl-CoA. These studies may be indicating that, in MCAD, Thr168 plays a role in preventing oxidation of the flavin by dioxygen. Although both acyl-CoA dehydrogenases and acyl-CoA oxidases perform the same reductive half-reaction (the α,*β*-dehydrogenation of acyl-CoA to *trans*-enoyl-CoA), the oxidative half-cycle (reoxidation of FAD) proceeds by two completely different routes. In the oxidative half-reaction, reduced FAD in acyl-CoA dehydrogenase is reoxidized by another group of flavoproteins known as electron transfer flavoprotein (ETF), closing the redox cycle. In contrast, this step is carried out by molecular oxygen in acyl-CoA oxidase (*2*).

In acyl-CoA oxidase, a glycine residue is in the same position as Thr168 in MCAD (*51*). This gives rise to a situation similar to that of the Thr168Ala mutant of the present study with respect to hydrogen-bonding patterns, but with a greater cavity. For acyl-CoA oxidase, the loss of hydrogen-bonding interaction between the threonine hydroxyl group and flavin N5, among other factors, is implicated to be responsible for an increase in the solvent-accessible surface area of the flavin ring that exposes it to the molecular oxygen (*51*). If the Thr168Ala mutation has an analogous effect, it will most likely affect the reoxidation of flavin by electron transfer flavoprotein (ETF) in the oxidative half-cycle. It is interesting to note that Thr168 also resides in the ETF binding site of MCAD (*2*).

*(C) Arg256Gln MCAD*. Although not directly involved in the chemical steps, the Arg256Gln mutation affects the hydrogen-bonding interactions of the thioester carbonyl group. Arg256 is instrumental in binding the substrate, octanoyl-CoA, through strong interactions with pantothenate carbonyls (CoA:O5 and CoA:O9 in Figure 5). In the Arg256Gln mutant, the Gln256 amide hydrogens are far from the substrate pantothenate group, and hence the strong interactions of arginine's guanidinium moiety with the substrate, observed in the wild-type case, are absent in this mutant. The failure to anchor the substrate in this mutant has an important effect on the geometry of the reaction center. In particular, it is reflected in very large changes in the two hydrogen-bonding interactions (CoA:O1*−FAD:H12′ and CoA:O1*−Glu376:HN) of the reaction center thioester carbonyl group (Figures 5−7 and Tables 1 and 2). Analysis of these hydrogen-bonding interactions along the reaction path indicates that both of them increase by 1−2 Å and are weakened as compared to the wild-type case. This makes the enolate transient species less stable as compared to the case of the wild-type enzyme or Thr168Ala MCAD. The backbone carbonyl of Glu376 makes a strong interaction with one of the Gln256 amide protons, with the Glu376:O−Gln256:HE12 distance varying from 1.9 to 2.5 Å. This analysis predicts that the binding of the octanoyl-CoA in the active site is severely compromised in this mutant. This is confirmed in the comparison of active site structures in the following subsection.

*Structural Changes in Thr168Ala and Arg256Gln MCAD*. Here we compare the following active site structural features in the two mutants to those in the wild-type enzyme: (i) the tricyclic isoalloxazine ring of FAD, (ii) the orientation of the thioester carbonyl (C1*−O1*) in octanoyl-CoA, (iii) the central part of the substrate which is anchored to the enzyme (by Arg256) through two pantothenate carbonyl oxygens (O5 and O9), and (iv) the phosphoadenosine tail of the substrate, which lies quite far (>15 Å) from the reaction center.

As described in the discussion of hydrogen-bonding interactions, for a particular enzyme these structural features do not show any significant change during the course of the two reactions. However, the active sites of the two mutants, Thr168Ala and Arg256Gln, do show some noticeable structural differences from the wild-type case all along the reaction paths. The wild-type active site is compared to those of Thr168Ala MCAD and Arg256Gln MCAD, shown in panels a and b of Figure 8, respectively. Only the respective proton transfer transition states are shown in this figure.

The absence of the threonine hydroxyl group in the Thr168Ala mutant reduces the interaction of Ala168 with the N5 and O4 atoms of the flavin ring as compared to the wild-type (Figure 4) and Arg256Gln MCAD. Consequently, the side of the flavin ring that interacts with Ala168 has undergone some changes compared to the wild-type enzyme. This is evident from the change in the local structure (inset of Figure 8a), containing atoms N3, C4, O4, and C4a. However, the position of the flavin ring relative to the substrate does not change much in the Thr168Ala MCAD case when compared to the wild-type enzyme. This is revealed from the average distance of the hydride acceptor atom, N5 (of FAD), to the hydride donor atom C3* (C*β*)

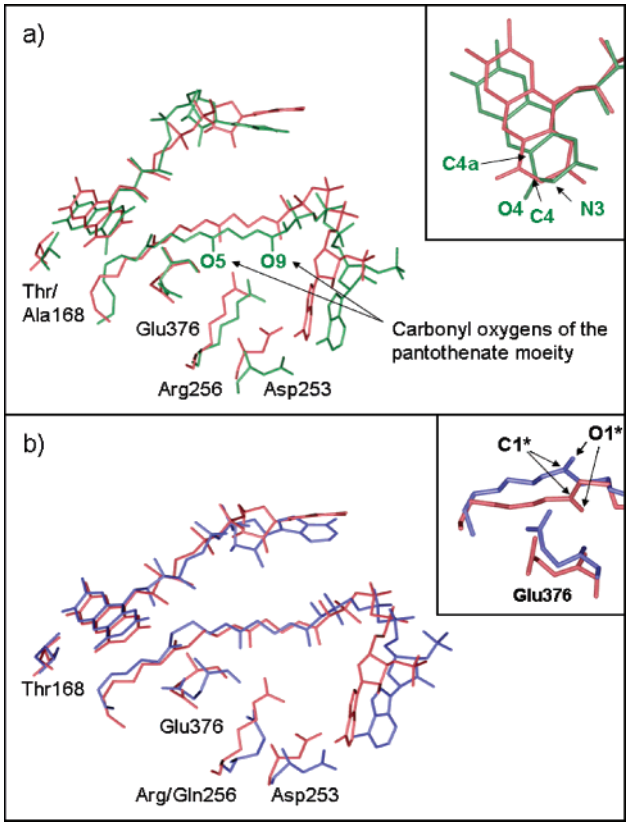


FIGURE 8: Relative orientation of the cofactor (FAD) and substrate (octanoyl-CoA) in the active site of the superimposed transition state structures of (a) wt (red) and Thr168Ala MCAD (green) and (b) wt (red) and Arg256Gln MCAD (blue). The insets show zoomed views of the orientations of (a) the cofactor flavin ring and (b) the substrate thioester carbonyl. Hydrogen atoms are omitted for clarity.

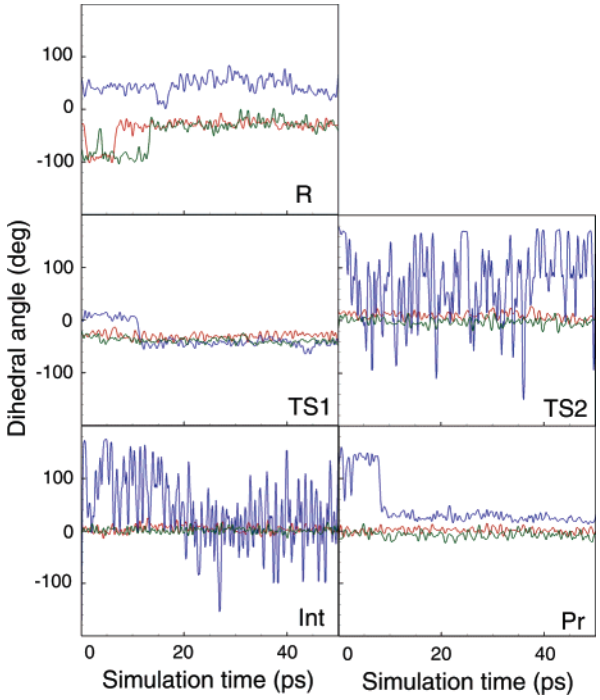


FIGURE 9: Comparative features of the fluctuations of the C3*−C2*−C1*−O1* torsional angles in the substrate along the two reaction coordinates for wt (red), Thr168Ala (green), and Arg256Gln MCAD (blue). The dihedral angles are plotted as functions of the simulation time. The reaction stages, indicated at the bottom right corner of each graph are labeled as follows: R (reactant), TS1 (proton transfer transition state), Int (intermediate), TS2 (hydride transfer transition state), and Pr (product).

(of octanoyl-CoA), which is about the same, 3.7 Å, in both wt and Thr168Ala MCAD. Also, the orientation of the thioester in this mutant remains superimposable on that in the wild-type enzyme (Figure 8a). There is some change in the interaction of Arg256 with the pantothenate carbonyl groups of the substrate. Unlike the wild-type enzyme, the positively charged guanidinium group of Arg256 resides in the middle of the two pantothenate carbonyls of the substrate and interacts with both of the oxygen atoms (O5 and O9). This structural change seems to have little influence on the energetics of either of the reaction steps. The entire phosphoadenosine group of the substrate in Thr168Ala MCAD appears to occupy a position slightly different from that observed in the wild type. The amide of the adenine group interacts strongly with Asp253, similar to the situation of the wild-type case, as observed in the hydrogen-bonding analysis.

In both wild-type and Thr168Ala MCAD, it was found that Arg256 acts as a primary anchoring residue for the substrate. In fact, the replacement of the positively charged arginine with a neutral glutamine results in complete loss of the interactions with the substrate. Throughout the two reaction steps, the nearest amide proton lies 5−8 Å away from the substrate pantothenate carbonyl oxygens, O5 and O9. This has been illustrated in Figure 8b by the superimposed transition state structure of the proton transfer step for the wt and Arg256Gln mutant. However, the consequence of this mutation is most noticeable in the change of the orientation of the thioester carbonyl relative to that in the wild-type and Thr168Ala mutant enzyme. In contrast to the wild-type structure the thioester C1*═O1* bond in this mutant is flipped about 180° with respect to the wild-type structure (inset of Figure 8b). This explains the longer hydrogen-bonding distances, observed for the O1* atom with Glu376:NH and FAD:H12′. Similar to the situation in Thr168Ala MCAD, the phosphoadenosine moiety of the substrate resides in a slightly different location compared to the wild-type enzyme.

The computational results predict that the Arg256Gln mutation severely affects the nature of substrate binding at the active site of the enzyme. The relevance of Arg256 in catalysis was observed independently by two other research groups (*44*, *52*) including a recent publication, while this paper was being reviewed (*52*). In both studies, mutations of this single residue completely destroyed the catalytic activity of this enzyme.

*Changes in the Dihedral Angles*. Because considerable double bond character is produced in the enolate ion transient species, the change in the dihedral angle (C3*−C2*−C1*−O1*) about the carbonyl carbon (C1*) and the Cα carbon (C2*) provides an indication of the progress of the two reaction steps, this dihedral angle is also a measure of the deformation of the substrate along the reaction path. At the conclusion of the second reaction step the C1*−C2* bond has full double-bond character, and the dihedral angle is zero. The evolution (for each of the three enzymatic catalysis) of this dihedral angle in the reactant (R), transition states (TS1 and TS2), and transient species (Int) to the product states (Pr) is shown in Figure 9.

For both wild type and Thr168Ala, the variation of the dihedral angles matches the expected behavior over the course of the reaction. In the reactant state, the C3*−C2*−C1*−O1* dihedral is nonzero and shows fluctuations in both directions as expected for the single-bonded character of C1*−C2*. As the reaction approaches the transient species state, the fluctuation decreases and the value of the dihedral angle oscillates around 0. This indicates that, after the abstraction of the α-proton from C1*, the anion is predominantly present in the enolate form and the transient species might be stabilized. In the hydride transfer step, no major change in this dihedral angle is noted; this indicates that, after a transient species is formed by the proton transfer, the hydride transfer does not require further rearrangement of the geometry and proceeds directly through the second transition state.

For Arg256Gln MCAD the dihedral angle (C3*−C2*−C1*−O1*) exhibits strong fluctuations at the end of the proton transfer reaction (Figure 9). The significant increase in oscillations of the dihedral angle is striking and is indicative of a highly fluxional state of the substrate molecule, precipitated by the proton abstraction from its C2* atom. Keeping in mind the differing orientation of the thioester carbonyl moiety (C1*−O1*) in the active site of this mutant as compared to that in the wild-type case, this observation further corroborates the loss of geometric requirements needed to stabilize the transient species in the enolate form. The fluctuations gradually reduce as the hydride transfer step progresses, and the average value of the dihedral angle reaches the range of 20−30°.

*Influence of Water Molecules on Catalysis*. To understand the role that solvent water plays in the *β*-oxidation, we monitored the fluctuations of the water molecules in the active site of MCAD. In the wild-type enzyme, we have identified and monitored water molecules that are within 5.0 Å of the thioester binding site, the specific base Glu376, or the flavin N5 nitrogen. We found that, by this definition, there are six water molecules. As the reaction propagates, the hydrogen-bonding distances of these water molecules, obtained as an average from the saved coordinates of MD simulations of a particular reaction stage, are given in Table 3.

In the thioester binding site a cluster of three water molecules, namely, W4, W422, and W3, interact with the ribityl 2′-hydroxyl group of FAD (FAD:O2′) and the thioester carbonyl oxygen (CoA:O1*). Two of these three water molecules, W3 and W4, are from the crystal structure. Besides these interactions they also interact with the neighboring pantothenate amide of octanoyl-CoA and the phosphate oxygen of FAD (data not shown). The hydrogen-bonding distances of the protons of these three water molecules were observed to be varying within 3−6 Å of the thioester binding site atoms, CoA:O1* and FAD:O2′. Knowing that the CoA, O1* atom, bears a uninegative charge after the proton transfer step, a comparison of these interacting distances were made in each stage of the catalysis (Table 3). It reveals that, for these two water molecules, designated as W3 and W4, the interacting distances drop significantly as the reaction passes through the transient species (Table 3). If the proton of W4 nearest to this site is designated as H2 and that of W3 as H1, then the decrease in the W4:H2−FAD:O2′ and W3:H1−FAD:O2′ distances in the transient species states are −1.4 and −0.3 Å, and −1.9 and −1.3 Å, respectively, as compared to those in the reactant and product states. The stronger hydrogen-bonding interaction associated with the transient species enolate speaks in favor of a significant role that these two water molecules might play in the catalysis.

Table 3: Comparison of the Hydrogen-Bonding Distances of Selected Water Molecules with the Reaction Center Thioester Carbonyl, Flavin Ring Nitrogen N5, Carboxylic Acid Group of Specific Base Glu376, and the Guanidinium Moiety of Arg256 in the Active Site of the Wild-Type Enzyme

| | α-proton abstraction and *β*-hydride transfer | | | | |
|---|---|---|---|---|---|
| interactions with water molecules | R (Å) | TS1 (Å) | Int (Å) | TS2 (Å) | Pr (Å) |
| FAD:O2′−W4:H2 | 4.6 | 4.3 | 3.2 | 3.3 | 3.5 |
| CoA:O1*−W4:H2 | 5.5 | 5.9 | 6.0 | 6.1 | 6.1 |
| FAD:O2′− W422:H1 | 3.4 | 4.2 | 3.7 | 2.7 | 2.8 |
| CoA:O1*−W422:H2 | 6.2 | 4.6 | 6.0 | 5.7 | 4.6 |
| FAD:O2′−W3:H1 | 4.9 | 4.6 | 3.0 | 4.8 | 4.3 |
| CoA:O1*−W3:H2 | 4.7 | 4.2 | 4.1 | 5.0 | 5.0 |
| E376:OE1−W1569:H2 | 1.8 | 1.9 | 3.1 | 3.8 | 3.0 |
| E376:OE1−W1569:H1 | 3.0 | 3.2 | 3.9 | 2.5 | 2.1 |
| R256:NE−W1559:H2 | 3.1 | 3.1 | 3.5 | 3.6 | 3.6 |
| R256:NH2−W1569:H2 | 3.8 | 3.8 | 4.0 | 4.0 | 4.5 |
| E376:OE2−W1447:H2 | 3.5 | 3.4 | 3.8 | 2.9 | 3.0 |
| R256:NE−W1447:H1 | 4.9 | 4.3 | 6.5 | 4.0 | 4.0 |
| R256:NH2−W1447:H2 | 5.8 | 5.4 | 6.0 | 5.0 | 4.6 |
| E376:OE1−W1447:H1 | 2.4 | 1.9 | 4.5 | 2.2 | 2.7 |
| FAD:O4−W2:OH2 | 2.2 | 2.0 | 2.0 | 3.1 | 2.0 |

The other water molecule, W422, has moderate-to-weak interactions with both FAD:O2′ and CoA:O1* atoms (Table 3). The proton abstracting base, Glu376, interacts with two other water molecules whose hydrogen atoms remain 2−3 Å away from the carboxylate oxygen. One of these water molecules also interacts with Arg256. Finally, the flavin oxygen (O4) is hydrogen bonded to a sixth water molecule [also observed in the crystal structure (*15*)], and this interaction is found to be maintained throughout the two catalytic steps (Table 3).

## CONCLUSIONS

For the wild-type acyl-CoA dehydrogenase as well as its two mutants, we found that the two C−H bond cleavages occur in a stepwise fashion via an enolate ion transient species, which is only 2−5 kcal/mol higher than the Michaelis complex. A similar result was obtained in the previous study of the short-chain enzyme (SCAD) (*10*) where a stepwise mechanism was predicted from simulated reaction steps. However, the present computation shows that in MCAD the difference between the energy barriers of the two reactions is smaller than that in the short-chain enzyme, the hydride transfer barrier being only 2 kcal/mol higher than that of the proton transfer. This indicates contributions of both of the two C−H bond dissociations in the rate-limiting process of this reaction. This is in contrast to the SCAD, where the *β*-hydride transfer reaction was predicted to be solely rate determining (*10*). In the present case, it might be possible to design experiments to perturb the system in a way that influences one catalytic step more than the other. This makes the catalytic mechanism in MCAD "tunable".

The disease-associated mutation of threonine 168 does not seem to have major effects on the catalysis. The computed free energy barrier is similar to that observed in the wild-type enzyme, although the relative barrier heights for the

proton and hydride transfer steps are reversed. This is consistent with experiments which showed that the Thr168Ala mutation only decreases the $k_{cat}$ value by 80% (*11*). Our calculation predicts 13%. Structural analysis of the Thr168Ala MCAD mutant reveals that the loss of one hydrogen bond has little effect on the orientation of the flavin ring. Also, the electrostatic charge decomposition analysis reveals that this residue does not have a significant effect on the energy profile along the reaction path. Thus the present study concludes that this residue plays an insignificant role in the enzyme catalysis in the reductive half-reaction, and the cause of the disease may be due to its effect in the subsequent reoxidation of flavin by ETF in the oxidative half-reaction.

Arginine 256 occupies a position at the center of a hydrogen-bonding network and is highly conserved in all of these enzymes. Crystal structural data show that it has two possible conformations in the active site. From the present study it is evident that only one specific conformation of this arginine residue is catalytically active. Simulation of the active site starting from the other conformation results in a catalytically inactive state of the enzyme. Furthermore, from these computations it can be concluded that this residue plays a very important role in catalysis. A model mutation performed by replacing this residue with glutamine causes significant damage to the hydrogen-bonding network near the arginine, which propagates a change in the bonding and orientation of the substrate reaction center. This mutation destroys two crucial hydrogen bonds between the substrate carbonyl and protein at the active site whose importance in stabilizing the enolate is well supported by experimental work (*48*). This work clearly shows that this results in a loss of orientation of the substrate and destabilization of both transition states, transient species, and product.

The computed potentials of mean force indicate that this arginine mutation has a pronounced effect on the hydride transfer step. A 10000-fold decrease of activity is predicted by this calculation for the Arg256Gln mutant, which implies that for all practical purposes this enzyme may be considered to be catalytically inactive. Our study further demonstrates that, besides binding, this arginine has a direct role in the stabilization of transient species and the two transition states. The hydrogen-bonding analysis clearly indicates that the loss of active site geometry because of this mutation plays a significant role in the destabilization of both transition states as well as the transient species between proton and hydride transfer steps.

Two independent research studies have recently been published with experimental results demonstrating the catalytic relevance of Arg256. As we were preparing this paper and assembling all of these results, Zeng et al. published the results of a study with the Arg256Gln MCAD mutant. Their experiments confirm a total loss of enzymatic activity (*44*). Furthermore, while this paper was being reviewed, another research article was published by O'Reilly et al., demonstrating the absolute importance of this residue in the catalysis (*52*).

The inconclusive nature of the KIE experiments has long kept the fundamental question about the mechanism of acyl-CoA dehydrogenases unanswered. Thus the observation of stepwise C−H bond breaking, as concluded from this study, bears considerable significance in the context of designing future experiments to further probe the mechanism. If the two enzymatic bond cleavages are fully nonconcerted, then the perturbation of any one C−H bond will not have an appreciable effect on the other. In that case experiments can be designed to quasi-independently change the relative barrier heights of the two steps. This may be accomplished, in principle, by introducing a modification in the substrate or in the enzyme. On the basis of this hypothesis one of the strategies being explored in this laboratory is to construct substrate analogues that can lower the proton transfer reaction barrier (or increase the hydride transfer reaction barrier). In particular, α-monofluoro- and γ,γ-difluoro-substituted derivatives of the octanoyl-CoA have already been synthesized and are currently being used to probe the enzyme mechanism (*53*).

The second approach arises from the catalytic role of Arg256 predicted by the present work and also subsequently confirmed by recent experimental findings by other researchers (*44*, *52*). The present computations show that a modification of the active site engineered by mutating this arginine (Arg256Gln) increases the hydride transfer reaction barrier, and as a result the reaction would stop after completion of only the proton transfer step. Consequently, this would provide us an opportunity to detect the transient species, if it is formed in the first step. Furthermore, since the arginine is absolutely conserved in the acyl-CoA dehydrogenase sequence (*12*), recently found to be associated with the MCAD deficiency disease (*52*), absolutely important in substrate binding (*16*), and has a proven role to influence the catalytic steps (*44*, *52*), the mutational substitution of this residue by neutral, charged, and hydrophobic residues can throw some light on the regulating aspects of this catalytic chemistry in this group of enzymes. The overexpression, purification, and characterization of one of the mutants (Arg248Ala) in the short-chain enzyme is currently being pursued (*54*) in this laboratory.

## ACKNOWLEDGMENT

We thank the University of Minnesota Supercomputing Institute for providing the necessary resources for performing the computations.

## REFERENCES

1. Vockley, J., and Whiteman, D. A. (2002) Defects of mitochondrial beta-oxidation: a growing group of disorders, *Neuromuscular Disord. 12*, 235−246.
2. Kim, J. J., and Miura, R. (2004) Acyl-CoA dehydrogenases and acyl-CoA oxidases. Structural basis for mechanistic similarities and differences, *Eur. J. Biochem. 271*, 483−493.
3. Rudik, I., Ghisla, S., and Thorpe, C. (1998) Protonic equilibria in the reductive half-reaction of the medium-chain acyl-CoA dehydrogenase, *Biochemistry 37*, 8437−8445.
4. Lenn, N. D., Stankovich, M. T., and Liu, H. W. (1990) Regulation of the redox potential of general acyl-CoA dehydrogenase by substrate binding, *Biochemistry 29*, 3709−3715.
5. Ghisla, S., and Thorpe, C. (2004) Acyl-CoA dehydrogenases. A mechanistic overview, *Eur. J. Biochem. 271*, 494−508.
6. Raichle, T. (1981) Ph.D. Thesis, Department of Chemistry, University of Konstanz, Konstanz, Federal Republic of Germany.
7. Murfin, W. W. (1974) Mechanism of the flavin reduction step in acyl CoA dehydrogenases, Ph.D. Thesis, Department of Chemistry, Washington University, St. Louis, MO.
8. Pohl, B., Raichle, T., and Ghisla, S. (1986) Studies on the reaction mechanism of general acyl-CoA dehydrogenase. Determination of selective isotope effects in the dehydrogenation of butyryl-CoA, *Eur. J. Biochem. 160*, 109−115.

9. Schopfer, L. M., Massey, V., Ghisla, S., and Thorpe, C. (1988) Oxidation−reduction of general acyl-CoA dehydrogenase by the butyryl-CoA/crotonyl-CoA couple. A new investigation of the rapid reaction kinetics, *Biochemistry 27*, 6599−6611.
10. Poulsen, T. D., Garcia-Viloca, M., Gao, J., and Truhlar, D. G. (2003) Free energy surface, reaction paths, and kinetic isotope effect of short-chain acyl-CoA dehydrogenase, *J. Phys. Chem. B 107*, 9567−9578.
11. Kuchler, B., Abdel-Ghany, A. G., Bross, P., Nandy, A., Rasched, I., and Ghisla, S. (1999) Biochemical characterization of a variant human medium-chain acyl-CoA dehydrogenase with a disease-associated mutation localized in the active site, *Biochem. J. 337* (Part 2), 225−230.
12. Bhattacharyya, S., Stankovich, M. T., and Gao, J. (2005) To explore long-range interactions in acyl-CoA dehydrogenases: a structural bioinformatics-based covariant mutation study, unpublished results.
13. Garcia-Viloca, M., Poulsen, T. D., Truhlar, D. G., and Gao, J. (2004) Sensitivity of molecular dynamics simulations to the choice of the X-ray structure used to model an enzymatic reaction, *Protein Sci. 13*, 2341−2354.
14. Lee, H. J., Wang, M., Paschke, R., Nandy, A., Ghisla, S., and Kim, J. J. (1996) Crystal structures of the wild type and the Glu376Gly/Thr255Glu mutant of human medium-chain acyl-CoA dehydrogenase: influence of the location of the catalytic base on substrate specificity, *Biochemistry 35*, 12412−12420.
15. Kim, J. J., Wang, M., and Paschke, R. (1993) Crystal structures of medium-chain acyl-CoA dehydrogenase from pig liver mitochondria with and without substrate, *Proc. Natl. Acad. Sci. U.S.A. 90*, 7523−7527.
16. Satoh, A., Nakajima, Y., Miyahara, I., Hirotsu, K., Tanaka, T., Nishina, Y., Shiga, K., Tamaoki, H., Setoyama, C., and Miura, R. (2003) Structure of the transition state analog of medium-chain acyl-CoA dehydrogenase. Crystallographic and molecular orbital studies on the charge-transfer complex of medium-chain acyl-CoA dehydrogenase with 3-thiaoctanoyl-CoA, *J. Biochem. (Tokyo) 134*, 297−304.
17. Gao, J., and Truhlar, D. G. (2002) Quantum mechanical methods for enzyme kinetics, *Annu. Rev. Phys. Chem. 53*, 467−505.
18. Gao, J., Amara, P., Alhambra, C., and Field, M. (1998) A generalized hybrid orbital (GHO) method for the treatment of boundary atoms in combined QM/MM calculations, *J. Phys. Chem. A 102*, 4714−4721.
19. Amara, P., Field, M., Alhambra, C., and Gao, J. (2000) The generalized hybrid orbital method for combined quantum mechanical/molecular mechanical calculations: formulation and tests of the analytical derivatives, *Theor. Chem. Acc. 104*, 336−343.
20. Alhambra, C., Wu, L., Zhang, Z.-Y., and Gao, J. (1998) Walden-inversion enforced transition state stabilization in a protein tyrosine phosphatase, *J. Am. Chem. Soc. 120*, 3858−3866.
21. Brooks, B. R., Bruccoleri, R. E., Olafson, B. D., States, D. J., and Swaminathan, S. J. (1983) CHARMM: A program for macromolecular energy, minimization, and dynamics calculations, *J. Comput. Chem. 4*, 187.
22. Pavelites, J. J., J., G., Bash, P. A., and MacKerell, A. D. J. (1997) A molecular mechanics force field for NAD + NADH, and the pyrophosphate groups of nucleotides, *J. Comput. Chem. 18*, 221−239.
23. MacKerell, A. D. J., Bashford, D., Bellott, M., Dunbrack, R. L. J., Evanseck, J. D., Field, M. J., Fischer, S., Gao, J., Gou, J., Ha, S., Joseph-McCarthy, D., Kuchnir, L., Kuczera, K., Lau, F. T. K., Mattos, C., Michnick, S., Ngo, T., Nguyen, D. T., Prodhom, B., Reiher, W. E. I., Roux, B., Schelenkrich, M., Smith, J. C., Stote, R., Straub, J., Watanbe, M., Wiórkiewicz-Kuczera, J., Yin, D., and Karplus, M. (1998) All-atom empirical potential for molecular modeling and dynamics studies of proteins, *J. Phys. Chem. B 102*, 3586−3616.
24. Jorgensen, W. L., Chandrasekhar, J., Madura, J. D., Impey, R. W., and Klein, M. L. (1983) Comparison of simple potential functions for simulating liquid water, *J. Chem. Phys. 79*, 926.
25. Rychaert, J. P., Ciotti, G., and Berensden, H. J. C. (1977) Numerical integration of the Cartesian equations of motion of a system with constraints: molecular dynamics of *n*-alkanes, *J. Comput. Phys. 23*, 327.
26. Hockney, R. W. (1970) The potential calculation and some applications, *Methods Comput. Phys. 9*, 136−211.
27. Verlet, L. (1967) Computer "experiments" on classical fluids. I. Thermodynamical properties of Lennard-Jones molecules, *Phys. Rev. 159*, 98−103.
28. Berman, H. M., Westbrook, J., Feng, Z., Gilliland, G., Bhat, T. N., Weissig, H., Shindyalov, I. N., and Bourne, P. E. (2000) The Protein Data Bank, *Nucleic Acids Res. 28*, 235−242.
29. Battaile, K. P., Molin-Case, J., Paschke, R., Wang, M., Bennett, D., Vockley, J., and Kim, J. J. (2002) Crystal structure of rat short chain acyl-CoA dehydrogenase complexed with acetoacetyl-CoA: comparison with other acyl-CoA dehydrogenases, *J. Biol. Chem. 277*, 12200−12207.
30. Dewar, M. J. S., Zoebisch, E. G., Healy, E. F., and Stewart, J. J. P. (1985) Development and use of quantum mechanical molecular models. 76. AM1: a new general purpose quantum mechanical molecular model, *J. Am. Chem. Soc. 107*, 3902.
31. Curtiss, L. A., Raghavachari, K., Redfern, P. C., Rassolov, V., and Pople, J. A. (1998) Gaussian-3 (G3) theory for molecules containing first and second-row atoms, *J. Chem. Phys. 109*, 7764.
32. Frisch, M. J., Trucks, G. W., Schlegel, H. B., Scuseria, G. E., Robb, M. A., Cheeseman, J. R., Montgomery, J. J. A., Vreven, T., Kudin, K. N., Burant, J. C., Millam, J. M., Iyengar, S. S., Tomasi, J., Barone, V., Mennucci, B., Cossi, M., Scalmani, G., Rega, N., Petersson, G. A., Nakatsuji, H., Hada, M., Ehara, M., Toyota, K., Fukuda, R., Hasegawa, J., Ishida, M., Nakajima, T., Honda, Y., Kitao, O., Nakai, H., Klene, M., Li, X., Knox, J. E., Hratchian, H. P., Cross, J. B., Bakken, V., Adamo, C., Jaramillo, J., Gomperts, R., Stratmann, R. E., Yazyev, O., Austin, A. J., Cammi, R., Pomelli, C., Ochterski, J. W., Ayala, P. Y., Morokuma, K., Voth, G. A., Salvador, P., Dannenberg, J. J., Zakrzewski, V. G., Dapprich, S., Daniels, A. D., Strain, M. C., Farkas, O., Malick, D. K., Rabuck, A. D., Raghavachari, K., Foresman, J. B., Ortiz, J. V., Cui, Q., Baboul, A. G., Clifford, S., Cioslowski, J., Stefanov, B. B., Liu, G., Liashenko, A., Piskorz, P., Komaromi, I., Martin, R. L., Fox, D. J., Keith, T., Al-Laham, M. A., Peng, C. Y., Nanayakkara, A., Challacombe, M., Gill, P. M. W., Johnson, B., Chen, W., Wong, M. W., Gonzalez, C., and Pople, J. A. (2004) *Gaussian 03*, Gaussian, Inc., Wallingford, CT.
33. Gonzalez-Lafont, A., Truong, T. N., and Truhlar, D. G. (1991) Direct dynamics calculations with NDDO (neglect of diatomic differential overlap) molecular orbital theory with specific reaction parameters, *J. Phys. Chem. 95*, 4618−4727.
34. Devi-Kesavan, L. S., Garcia-Viloca, M., and Gao, J. (2003) Semiempirical QM/MM potential with simple valence bond (SVB) for enzyme reactions. Application to the nucleophilic addition reaction in haloalkane dehalogenase, *Theor. Chem. Acc. 109*, 133.
35. Brooks, C. L., III, Brunger, A., and Karplus, M. (1985) Active site dynamics in protein molecules: a stochastic boundary molecular-dynamics approach, *Biopolymers 24*, 843−865.
36. Kumar, S., Swendsen, R. H., Kollman, P. A., and Rosenberg, J. M. (1992) The weighted histogram analysis method for free energy calculations on biomolecules, *J. Comput. Chem. 13*, 1011.
37. Boczko, E. M., and Brooks, C. L. (1993) Constant-temperature free energy surfaces for physical and chemical processes, *J. Phys. Chem. 97*, 4509−4513.
38. Rajamani, R., Naidoo, K. J., and Gao, J. (2003) Implementation of an adaptive umbrella sampling method for the calculation of multidimensional potential of mean force of chemical reactions in solution, *J. Comput. Chem. 24*, 1775−1781.
39. Kim, J. J., and Wu, J. (1988) Structure of the medium-chain acyl-CoA dehydrogenase from pig liver mitochondria at 3-A resolution, *Proc. Natl. Acad. Sci. U.S.A. 85*, 6677−6681.
40. Djordjevic, S., Pace, C. P., Stankovich, M. T., and Kim, J. J. (1995) Three-dimensional structure of butyryl-CoA dehydrogenase from *Megasphaera elsdenii*, *Biochemistry 34*, 2163−2171.
41. Bhattacharyya, S., Stankovich, M. T., and Gao, J. (2005) Molecular simulation of acyl-CoA dehydrogenases, unpublished results.
42. Hu, W.-P., and Truhlar, D. G. (1996) Factors affecting competitive ion−molecule reactions: $ClO^- + C_2H_5Cl$ and $C_2D_5Cl$ via $E_2$ and $SN_2$ channels, *J. Am. Chem. Soc. 118*, 860−869.
43. Garrett, B. C., and Truhlar, D. G. (1982) New semiempirical method of modeling potential energy surfaces for generalized TST and application to the kinetic isotope effects in the chlorine−hydrogen−hydrogen system, *J. Chem. Phys. 76*, 1853−1858.
44. Zeng, J., and Li, D. (2004) Expression and purification of His-tagged rat mitochondrial medium-chain acyl-CoA dehydrogenase wild-type and Arg256 mutant proteins, *Protein Expression Purif. 37*, 472−478.
45. Nishina, Y., Sato, K., Hazekawa, I., and Shiga, K. (1995) Structural modulation of 2-enoyl-CoA bound to reduced acyl-CoA dehydrogenases: a resonance Raman study of a catalytic intermediate, *J. Biochem. (Tokyo) 117*, 800−808.

46. Johnson, B. D., Mancini-Samuelson, G. J., and Stankovich, M. T. (1995) Effect of transition-state analogues on the redox properties of medium-chain acyl-CoA dehydrogenase, *Biochemistry 34*, 7047−7055.
47. Engst, S., Vock, P., Wang, M., Kim, J.-J. P., and Ghisla, S. (1999) Mechanism of activation of acyl-CoA substrates by medium chain acyl-CoA dehydrogenase: interaction of the thioester carbonyl with the flavin adenine dinucleotide ribityl side chain, *Biochemistry 38*, 257−267.
48. Wu, J., Bell, A. F., Luo, L., Stephens, A. W., Stankovich, M. T., and Tonge, P. J. (2003) Probing hydrogen-bonding interactions in the active site of medium-chain acyl-CoA dehydrogenase using Raman spectroscopy, *Biochemistry 42*, 11846−11856.
49. Saijo, T., and Tanaka, K. (1995) Isoalloxazine ring of FAD is required for the formation of the core in the Hsp60-assisted folding of medium chain acyl-CoA dehydrogenase subunit into the assembly competent conformation in mitochondria, *J. Biol. Chem. 270*, 1899−1907.
50. Matthews, D. A., Alden, R. A., Birktoft, J. J., Freer, S. T., and Kraut, J. (1975) X-ray crystallographic study of boronic acid adducts with subtilisin BPN′ (Novo). A model for the catalytic transition state, *J. Biol. Chem. 250*, 7120−7126.
51. Nakajima, Y., Miyahara, I., Hirotsu, K., Nishina, Y., Shiga, K., Setoyama, C., Tamaoki, H., and Miura, R. (2002) Three-dimensional structure of the flavoenzyme acyl-CoA oxidase-II from rat liver, the peroxisomal counterpart of mitochondrial acyl-CoA dehydrogenase, *J. Biochem. (Tokyo) 131*, 365−374.
52. O'Reilly, L. P., Andresen, B. S., and Engel, P. C. (2005) Two novel variants of human medium chain acyl-CoA dehydrogenase (MCAD), *FEBS J. 272*, 4549−4557.
53. Stankovich, M. T., Luo, L., Holt, E., Nelsen, A., Brenner, M., Bhattacharyya, S., Jheng, H., and Lipscomb, J. (2005) Probing the acyl-CoA dehydrogenase mechanism using fluorinated substrates, unpublished results.
54. Nelsen, A., Bhattacharyya, S., Gao, J., and Stankovich, M. T. (2005) Uncovering the reaction mechanism of acyl-CoA dehydrogenases: overexpression and characterization of a highly conserved Arg248 mutants of short chain enzyme, unpublished results.

BI051630M